Diagnostic Overview for Non-solenoidal Startup Experiments on PEGASUS-III

PEGASUS-III Experiment

M.D. Nornberg, M.W. Aslin, M.W. Bongard, M.T. Borchardt, S.J. Diem, A.L. Ferris, R.J. Fonck, J.A. Goetz, A.K. Keyhani, B.A. Kujak-Ford, B.T. Lewicki, J.K. Peery, C. Pierren, J.A. Reusch, A.T. Rhodes, C. Rodriguez Sanchez, R.K. Sassella, C.E. Schaefer, A.C. Sontag, T.N. Tierney, J.D. Weberski, G.R. Winz

Department of Engineering Physics
UNIVERSITY OF WISCONSIN–MADISON

64th Annual Meeting of the APS Division of Plasma Physics, Spokane, WA, Presentation CP11.00046, 17 October 2022

Work supported by US DOE Grants DE-SC0019008 and DE-SC0020402

PEGASUS-III: A Dedicated Platform for Solenoid-Free Startup

- Develop solenoid-free startup in a dedicated facility
  - Local Helicity Injection (LHI)
  - Coaxial Helicity Injection (CHI: Transient, Sustained)
  - RF assist and sustainment (EBW, ECH, ECCD)
  - Assess compatibility with RF/NBI heating and current drive
- Goal: develop validated physics and technology basis for MA-class startup

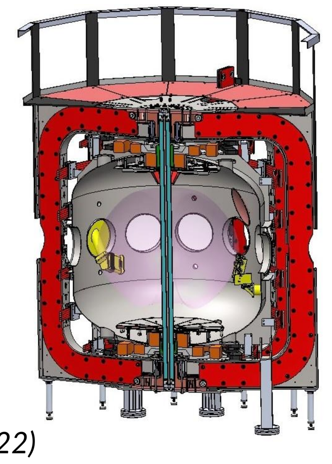

A. C. Sontag et al., IEEE Trans. Plasma Sci. (2022)
Bongard CP11.00040

Diagnostic Needs for Solenoid-Free Startup Studies

Equilibrium & Kinetic profiles	MHD turbulence & relaxation	Impurity content	Source characterization

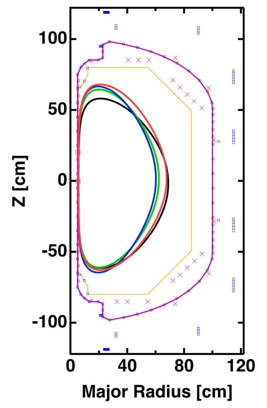

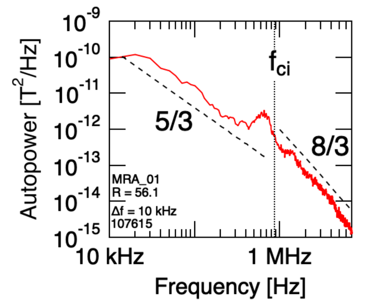

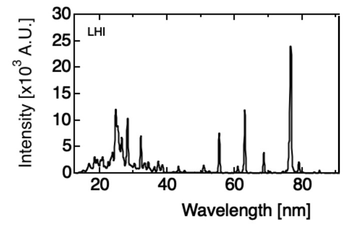

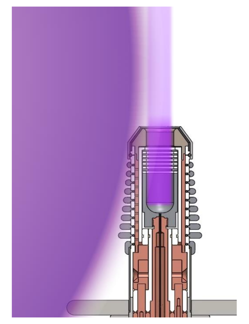

Magnetic Equilibrium Reconstruction

Sensor placement optimized using sensitivity analysis of reconstructions

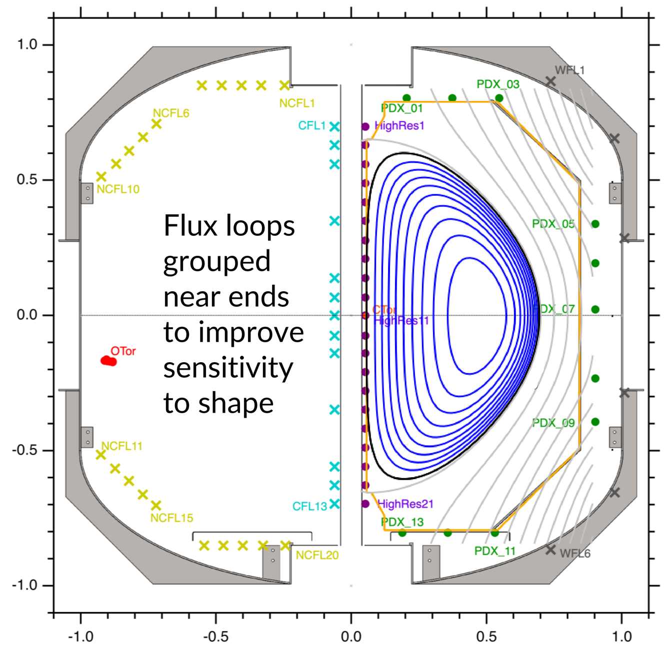

Diagnostic	Number
Rogowski coils	2
Diamagnetic loops	3
Poloidal Mirnov array	32
Toroidal Mirnov array	12
Centerstack flux loops	13
Internal flux loops	20
Wall flux loops	6

Center stack diagnostics fit within 8 mm gap

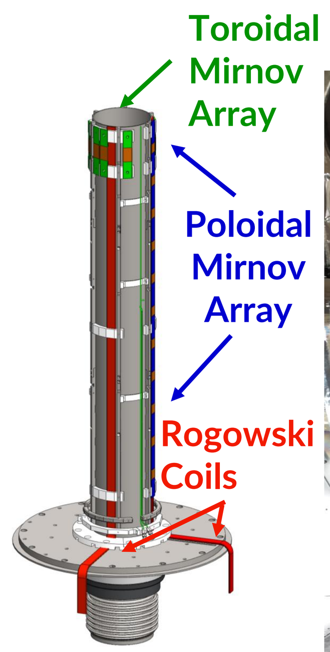

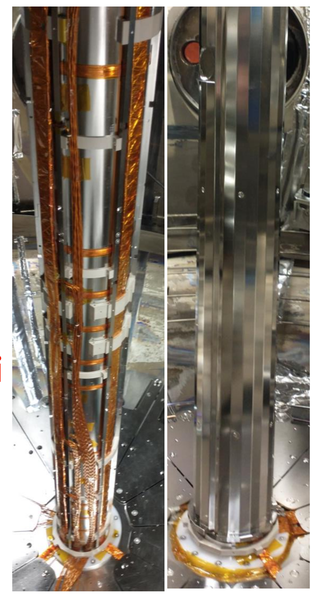

Mirnov Coil alignment improved
- Array mounted to standalone structure
- 2 arcmin alignment tolerance

Signal electronics robust to EMI
- Flux loops and Mirnov coils shielded
- Shielded CAT7 twisted-pair
- Balanced input into 80 dB differential amp
- 200 kHz 8-pole filter (bit-level antialiasing)
- 1 MHz ADC

Kinetic Profile Measurements

Helicity injection requires magnetic relaxation
- Heats both ions and electrons
- Localized to the plasma edge
- Results in low inductance plasmas

Motivates core pressure measurements:
- Thomson Scattering
- Interferometry
- Diagnostic Neutral Beam
- Charge Exchange Spectroscopy

Thomson Scattering Pressure profiles

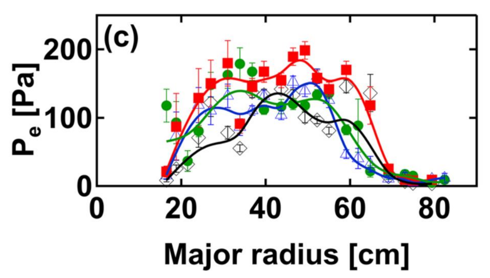

Bodner, et al., Phys Plasmas **28**, 102504 (2021)

Thomson Scattering (see CP11.00051)
Single pulse 2 J Nd:YAG Laser
2nd harmonic amplifier (532 nm)
Automated mirror alignment
In vacuuo baffles for stray light
24 channel collection optics
Holographic transmission grating (80%)
ICCD camera with custom fast shutters

Charge Exchange Recombination Spectroscopy
Under design (see *Keyhani CP11.00052*)
10 channels collection optics
Holographic transmission grating
sCMOS camera for kHz acquisition

Microwave Heterodyne Interferometer
288 GHz (mm-wave) source
New center stack mirror
(reduces refraction)

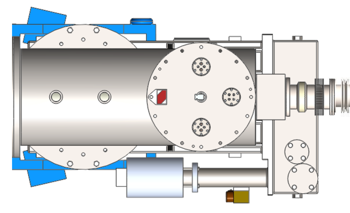

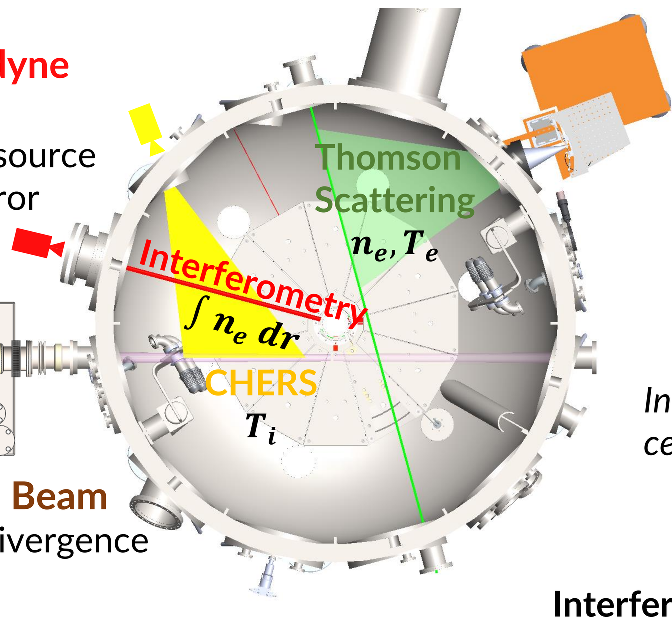

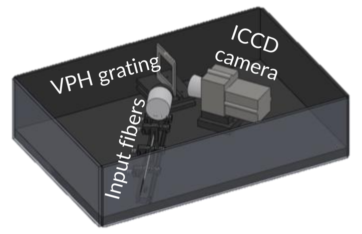

Diagnostic Neutral Beam
80 kV with 9 mrad divergence
100 msec pulse
Arc plasma source
(optimized energy fraction)

Interferometer mirror on center stack reduces refraction

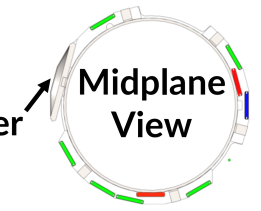

Quantifying Impact of Impurities on Startup

Impurities impact helicity injection:
- Increase Z_{eff}
- Radiative cooling increases P_{rad}
- Increase resistivity $\eta \propto Z_{eff} T_e^{-3/2}$

Diagnostics to quantify impurities:
- Radiometry (AXUV diode array)
- VUV spectroscopy (SPRED)
- Visual Bremsstrahlung (VB)

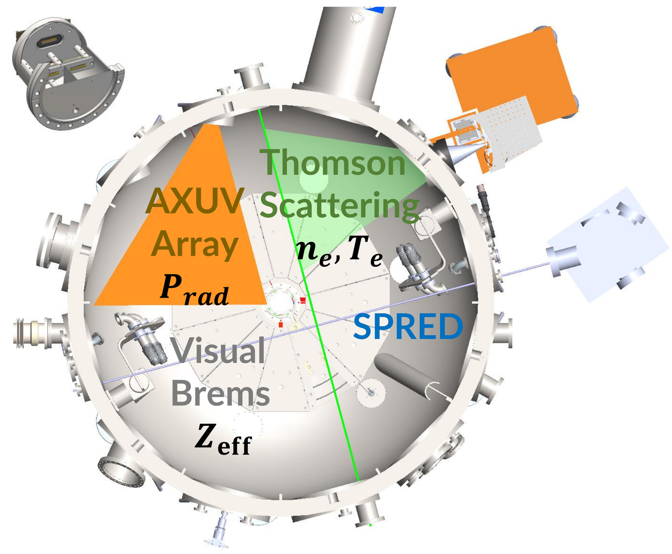

Quantifying impurity transport critical to Z_{eff} and P_{rad} calculations
- Charge state profiles depend on transport
- Collisional radiative transport modelling with STRAHL
- Constrain with VB, P_{rad} measurements

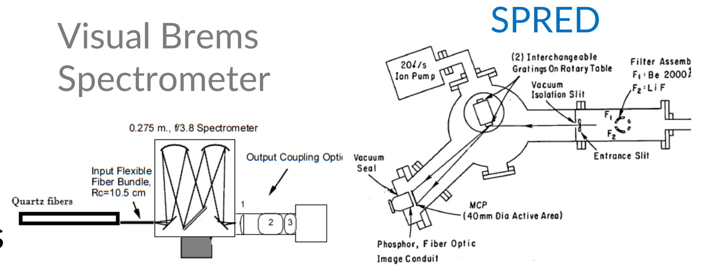

See Rodriguez Sanchez CP11.00050

Resolve short-wavelength VUV emission with high resolution grating

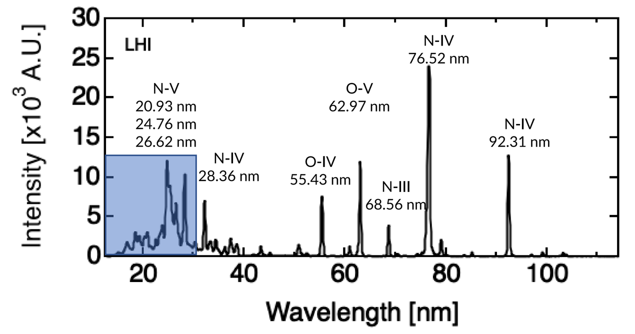

Z_{eff} dependent on impurity transport

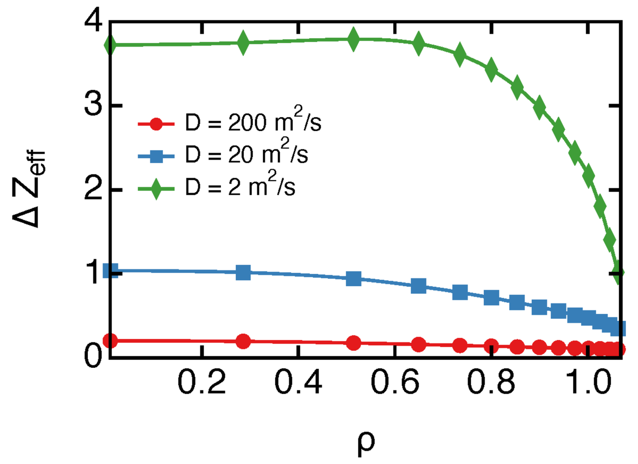

Injector Impedance Depends on Arc Density

Biasing the injector creates double layer
- Rapid potential drop over λ_{Debye} accelerates electrons
- Circuit impedance depends on arc density and plasma edge density

Injector shape optimization → extended aperture along flux surface
How is this double layer affected by changes in aspect ratio?
- Can we generate a homogenous arc plasma in extended aperture injector?
- Quantify arc density using multipoint Stark Broadening measurement

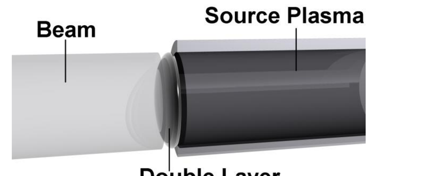

Hinson, *et al.*, Phys Plasmas **23**, 052515 (2016))

Non-circular Injector

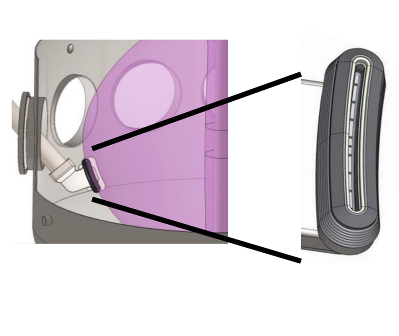

Collection optics array and spot size matched to injector

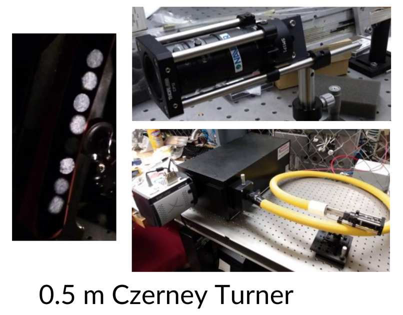

0.5 m Czerney Turner Spectrometer EMCCD camera

Predicted lines shape show good sensitivity for expected density

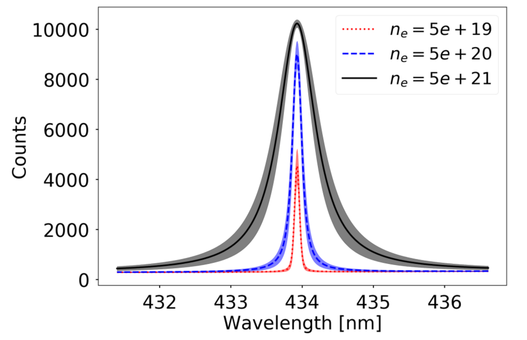

CHI Efficiency Depends on Flux Footprint Separation

Additional flux loops used to measure flux footprint separation

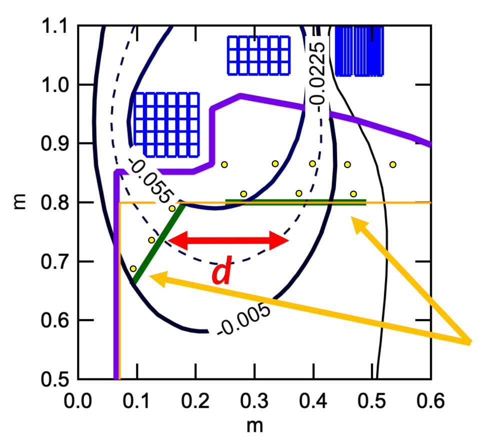

Flux loops added to electrodes to measure d

Divertor coils enable variation in flux distribution
- Rate of helicity injection depends on geometry
- Smaller distance between electrodes facilitates:
  - Stronger flux expulsion from $\boldsymbol{J}_R \times \boldsymbol{B}_t$ force
  - Faster rate of reconnection in current sheet
- Vary flux footprint width d at constant ψ_{inj}
- Test scaling of flux conversion efficiency

See Reusch CP11.00044

Microwave Emission Measurements for EBW

Display of Vivaldi antennas used in SAMI

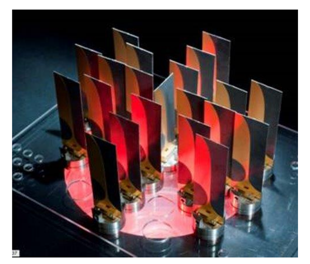

First measurements of EBW emitted from LHI plasmas
- Plasma acts as blackbody
- Waves generated spontaneously by plasma fluctuations
- Electron Bernstein Waves emitted via BXO mode conversion
- Measurement using Synthetic Aperture Microwave Imaging
- Informs RF current drive system design

See Peery CP11.00042

Magnetic Relaxation and Current Drive Facilitated by Alfvénic Turbulence

Several insertable probe arrays are used to characterize $\tilde{\boldsymbol{B}}$

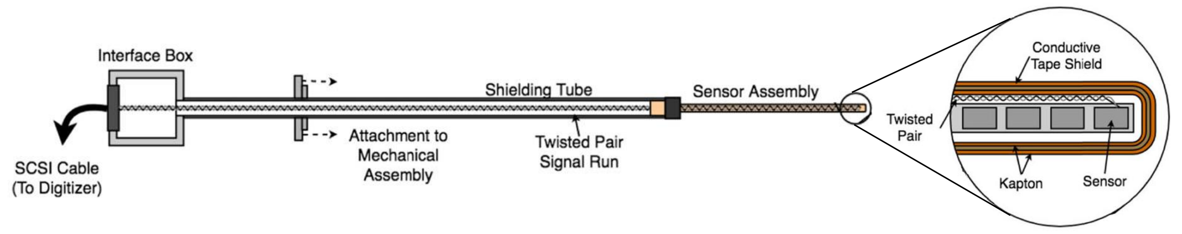

- Radial Triplet Array Probe
  - Measures $\dot{\boldsymbol{B}}(R,t)$
  - 10 radial locations
  - $\Delta R \sim 1$ cm $\sim \rho_s$
  - 6 MHz frequency resolution

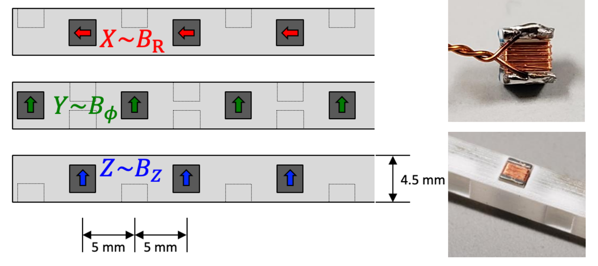

- Radial Hall Probe Array
  - Measures $\boldsymbol{B}(R,t)$
  - 8 radial locations
  - $\Delta R \sim 1$ cm $\sim \rho_s$
  - 6 MHz frequency resolution

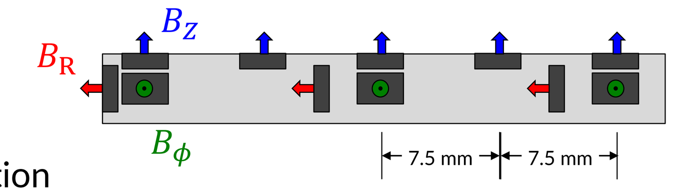

Richner, et al., *Rev. Sci. Instr.* **89**, 10J103 (2018)

Alfvénic turbulence driven by e-beam instabilities

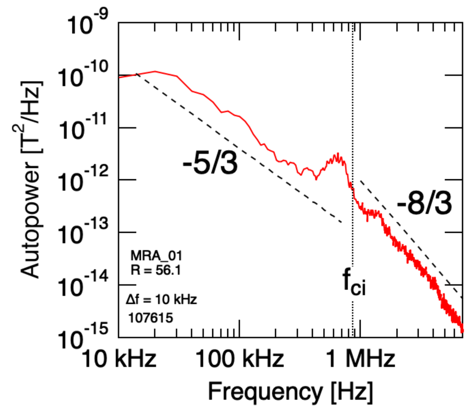

Dynamo EMFs responsible for current drive

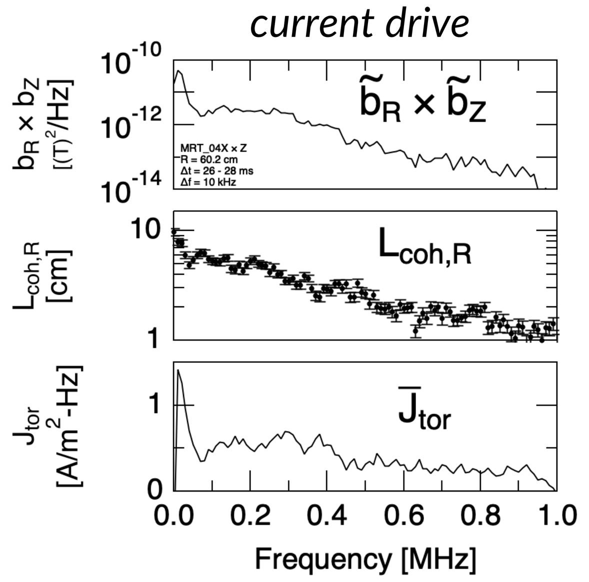

$\int \tilde{J}_{tor}(f) df \approx$ 400 kA/m² ~ $\langle J_{tor}\rangle$

Richner, et al., Phys. Rev. Lett. **128**, 105001 (2022)

Alfvenic turbulence facilitates magnetic relaxation to tokamak
- Establish that mechanisms scale to MA-class startup
- Identify location of instability
- Explore role of anisotropy in relaxation
- Scaling with B_T, n_e, and V_{inj}

See R. Sassella CP11.00048

PEGASUS-III Diagnostics for Non-Solenoidal Startup

Diagnostics based on mission-critical requirements
- Kinetic equilibrium reconstruction
- MHD activity associated with relaxation
- Impurity content & transport
- Characterizing current drive sources

New systems being deployed:
- Neutral Beam diagnostics (CHERS)
- Higher-resolution VUV spectroscopy
- Higher throughput Visual Brems
- Arc plasma density (Stark Broadening)
- Microwave imaging of EBW emission

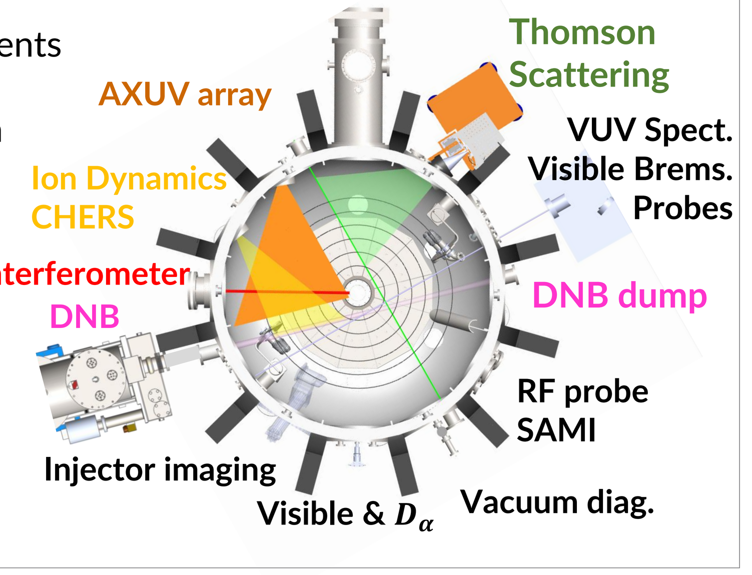

Reprints available at https://pegasus.ep.wisc.edu/technical-reports.